Transport properties of an intermediate-valence model of $Tl_2Mn_2O_7$

M. E. Foglio and G. E. Barberis
Instituto de Física "Gleb Wataghin," UNICAMP, 13083-970, Campinas, São Paulo, Brazil
(Received 14 November 2004; revised manuscript received 2 August 2005; published 30 September 2005)

The appearance of colossal magnetoresistance (CMR) in $Tl_2Mn_2O_7$ has stimulated many recent studies of the pyrochlore family of compounds $A_2B_2O_7$. The double exchange model of Zener does not describe the CMR in $Tl_2Mn_2O_7$, because its metallic conductivity cannot be explained by doping. Here we employ Hubbard operators to reformulate the intermediate valence model used by Ventura and Alascio [Phys. Rev. B **56**, 14533 (1997)] to describe the electronic structure and transport properties of this compound. Following Foglio and Figueira [Phys. Rev. B **62**, 7882, (2000)] we use approximate one-electron Green's functions to calculate the thermopower and the static and dynamic conductivity of $Tl_2Mn_2O_7$ for several magnetic fields. A qualitative agreement was obtained with the experimental measurements of those properties. Although the agreement is far from perfect, these quantities are fairly well described by the same set of system parameters.

DOI: 10.1103/PhysRevB.72.125129 PACS number(s): 71.10.Fd, 75.47.Gk, 72.15.Jf, 71.27.+a

I. INTRODUCTION

The $A_2B_2O_7$ pyrochlore family of compounds has been the object of many recent studies, principally because of the appearance of colossal magnetoresistance (CMR) in the $Tl_2Mn_2O_7$ compound. This material was reported as ferromagnetic, metallic, and with enormous negative magnetoresistance in the region of temperatures corresponding to the ferromagnetic transition ($T_c \sim 120$ K). The principal interest created for this material is that the double exchange (DE) Zener model does not explain the CMR in this material. Experimental studies show that, when compared with other $A_2Mn_2O_7$ compounds, the Tl one is unique. It has a very high T_c, a property shared with the In pyrochlore, but it is the only compound of the series that presents metallic conductivity, which cannot be explained by doping because it is present in the stoichiometric compound. Several recent band calculations[1–3] show that the material is expected to be almost half metallic at low temperatures, that is, the conductivity is driven within only one of the spin directions. This property is the same for the DE perovskites, but in that case the conductivity and the ferromagnetism appear only with doping.

The whole family of Mn pyrochlores shows ferromagnetism,[4] and their bands present similarities, with a band gap reducing its value from Y to Tl, where the compound is slightly metallic with very different conductivity for both spin directions. The ferromagnetism in the Mn pyrochlore compounds is explained by the Kanamori-Goodenough rules, as the result of superexchange through the O ligands. However, the Curie temperatures do not scale with the bond angles, which seems to indicate a different mechanism for the In and Tl compounds[4] (the calculated values of the exchange parameter J for the Tl, In, and Y compounds are, respectively, 0.11, 2.52, and 1.1 K, but their corresponding measured T_c's are 124, 129, and 16 K).

The experimental paper published by Raju *et al.*[5] tries to explain the ferromagnetism of the Tl compound through DE, but several evidences proved afterward that the origin of ferromagnetism is only superexchange.

A small number of carriers, of the order found in doped semiconductors [$\sim 10^{19}$ cm^{-3}], was found in the Tl compound by measuring Hall effect.[6] Several authors obtain a large enhancement of the magnetoresistance[1,7] by doping the Tl sites with In and Sc, or the Mn sites with Ru. The behavior of the resistivity is sample dependent[6,8] at high T, which created a controversy about the compound's behavior in this region of temperatures.

Imai *et al.*[9] present the more complete set of measurements of Hall effect and magneto-thermopower. They measured the anomalous Hall coefficient at low (below T_c) and high temperatures, and they found it small in both cases. Following Singh[3] they assume a very simple quasispherical Fermi surface and fit the thermopower to the effective mass model.

Increasing the pressure reduces the value of T_c for all the Mn pyrochlores.[10] Nuñez-Regueiro and Lacroix[11] developed a theory for this effect that gives good agreement with the experimental results, confirming that the ferromagnetism is due to superexchange.

Ventura and Alascio[12] used an intermediate valence (IV) model for the Tl, and they could explain both the conductivity and the CMR of the pure Tl compound. Here we refine their calculations, using the same IV model but employing Hubbard X operators.[13] We calculated both the static and dynamic conductivity, obtaining a qualitative agreement with the measured quantities[14,15] without having to assume an O deficiency. This agrees with the result of the published band studies.[1–3] Following Schweitzer and Czycholl[16] we calculate the thermopower and magnetothermopower, and our results agree with the experiments.[9]

In Sec. II we reformulate the model of Ventura and Alascio, employing the Hubbard operators. We discuss the approximate GF that we employ in the calculation, and give the formulas to calculate the resistivity, optical conductivity, and thermopower. In Sec. III we discuss the parameters we shall use and calculate the transport properties, and in Sec. IV we present our conclusions. Finally, we give the atomic states employed to calculate the GF in Appendix A and a discussion about the resistivity mechanism in Appendix B.

II. MODEL WITH *X*-OPERATORS

The model employed[12] is a lattice of local states hybridized with a conduction band. Each local state has two magnetic configurations with spin $S=1/2$ and $S=1$, respectively, that are hybridized with the conduction electrons. The local state with $S_z=0$ of the $S=1$ configuration is discarded, so that we have two independent systems with spin up and spin down, respectively, because the hybridization conserves the spin direction. Each local site j has then two states $|j,\sigma\rangle$ with $S=\frac{1}{2}$, $\sigma=\pm\frac{1}{2}$ and two states $|j,s\rangle$ with $S=1$, $s=\pm 1$, and their respective energies are E_σ and E_s.

We can assume arbitrary properties and energies for the relevant localized states of this model, and it is then convenient to describe them employing Hubbard operators $X_{j;a,b}=|j,a\rangle\langle j,b|$, which transform the state $|j,b\rangle$ into the state $|j,a\rangle$, i.e., $X_{j,ab}|j,b\rangle=|j,a\rangle$. These operators do not satisfy Wick's theorem, and one uses instead their product rules at the same site

$$X_{j,ab}X_{j,cd}=\delta_{b,c}X_{j,ad}. \tag{1}$$

When the operators are at different sites we chose properties equivalent to those of the usual Fermi or Bose: We say that $X_{j,ab}$ is of the "Fermi type" ("Bose type") when the number of electrons in the two states $|j,a\rangle$ and $|j,b\rangle$ differ by an odd (even) number. For $j\neq j'$ we then use $\{X_{j,ab},X_{j',cd}\}=0$ when the two operators are of the "Fermi type" and $[X_{j,ab},X_{j',cd}]=0$ when at least one is of the "Bose type" (as usual,[17] $[a,b]=ab-ba$ and $\{a,b\}=ab+ba$).

We then write the model's Hamiltonian

$$H=\sum_{j,\sigma}E_\sigma X_{j;\sigma\sigma}+\sum_{j,s}E_s X_{j;ss}+\sum_{\mathbf{k},\sigma}E_{\mathbf{k},\sigma}c^\dagger_{\mathbf{k},\sigma}c_{\mathbf{k},\sigma}+\sum_{j,\mathbf{k},\sigma}(V_{j,\mathbf{k},\sigma}X^\dagger_{j;\sigma,s=2\sigma}c_{\mathbf{k},\sigma}+V^*_{j,\mathbf{k},\sigma}c^\dagger_{\mathbf{k},\sigma}X_{j;\sigma,s=2\sigma}), \tag{2}$$

where we denote the Hubbard operators $X_{j;\pm\frac{1}{2},\pm 1}$ with $X_{j;\sigma,s=2\sigma}$ (note that $X_{j;b,a}=X^\dagger_{j;a,b}$). The $c^\dagger_{\mathbf{k},\sigma}$ and $c_{\mathbf{k},\sigma}$ are the creation and destruction operators of a conduction electron with energies $E_{\mathbf{k},\sigma}$, wave vector $\mathbf{k}$, and spin component $\sigma\hbar/2$, where $\sigma=\pm 1$. The hybridization constant is

$$V_{j,\mathbf{k},\sigma}=(1/\sqrt{N_s})V(\mathbf{k})\exp(i\mathbf{k}\cdot\mathbf{R_j}), \tag{3}$$

where N_s is the number of sites, and $V(\mathbf{k})$ is independent of $\mathbf{k}$ when the mixing is purely local.

The cumulant expansion was extended by Hubbard[18] to study a quantum problem with fermions, and he derived a diagrammatic expansion involving unrestricted lattice sums of connected diagrams that satisfies a linked cluster theorem. The extension of this technique to the Anderson lattice[19] is sufficiently general to treat the model described by Eq. (2), and it is the basis of the present treatment. One has to use the Grand Canonical Ensemble of electrons, and it is then convenient to introduce

$$\mathcal{H}=H-\mu\left\{\sum_{\vec{k},\sigma}C^\dagger_{\vec{k},\sigma}C_{\vec{k},\sigma}+\sum_{ja}\nu_a X_{j,aa}\right\}, \tag{4}$$

where μ is the chemical potential and ν_a is the number of electrons in the state $|j,a\rangle$, and without any restriction for the treatment we shall use $\nu_{\pm\frac{1}{2}}=0$ and $\nu_{\pm 1}=1$. It is also convenient to introduce

$$\varepsilon_{j,a}=E_{j,a}-\mu\ \nu_a, \tag{5}$$

$$\varepsilon_{\mathbf{k}\boldsymbol{\sigma}}=E_{\mathbf{k}\boldsymbol{\sigma}}-\mu, \tag{6}$$

because these are the expressions that appear consistently in the calculations.

The last term in Eq. (2) will be considered as the perturbation, and the exact and unperturbed averages of any operator A shall be, respectively, denoted by $\langle A\rangle_{\mathcal{H}}$ and $\langle A\rangle$.

A. Approximate Green's functions

As in the Anderson lattice[13] with $U\to\infty$ one can introduce one-particle Green's functions (GFs) of local electrons

$$\langle[X_{j;\sigma,s=2\sigma}(\tau)X^\dagger_{j;\sigma,s=2\sigma}(\tau')]_+\rangle_{\mathcal{H}}, \tag{7}$$

as well as GFs for the conduction electrons $\langle[C_{k\sigma}(\tau)C^\dagger_{k'\sigma}(\tau')]_+\rangle_{\mathcal{H}}$ and "crossed" GFs of the type $\langle[X_{j;\sigma,s=2\sigma}(\tau)C^\dagger_{k'\sigma}(\tau')]_+\rangle_{\mathcal{H}}$, all of them defined in the intervals $0\leqslant\tau$, $\tau'\leqslant\beta\equiv 1/T$. It is possible to associate a Fourier series to these GFs because of their boundary condition in this variable,[19] and the coefficients $\langle[X_{j;\sigma,s=2\sigma}(\omega_\nu)X^\dagger_{j;\sigma,s=2\sigma}(\omega_{\nu'})]_+\rangle_{\mathcal{H}}$ correspond to the Matsubara frequencies $\omega_\nu=\pi\nu/\beta$ (where ν are all the positive and negative odd integer numbers). One can also transform the GF to reciprocal space,[19] and because of the invariance against time and lattice translations

$$\langle[X_{j;\sigma,s=2\sigma}(\omega_\nu)X^\dagger_{j;\sigma,s=2\sigma}(\omega_{\nu'})]_+\rangle_{\mathcal{H}}=G_{ff,\sigma}(\mathbf{k},\omega_\nu)\delta_{\mathbf{k}',\mathbf{k}}\delta_{\nu+\nu',0}. \tag{8}$$

Transforming the eigenstates of the c electrons to the Wannier representation, one also obtains the equivalent relations for $G_{cc,\sigma}(\mathbf{k},\omega_\nu)$ and $G_{fc,\sigma}(\mathbf{k},\omega_\nu)$. Considering that the coefficients of the τ Fourier series for each $\mathbf{k}$ are the values of a function of the complex variable $z=\omega+iy$ at the points $z_\nu=i\omega_\nu$, it is possible to make the analytical continuation to the upper and lower half-planes of z in the usual way,[20] obtaining, e.g., from the $G_{ff,\sigma}(\mathbf{k},\omega_\nu)$, a function $G_{ff,\sigma}(\mathbf{k},z)$ which is minus the Fourier transform of the double time GF.[21]

The one-electron GF of ordinary fermions or bosons can be expressed as a sum of infinite "proper" (or irreducible) diagrams,[17] and a similar result was obtained for the Hubbard model employing the cumulant expansion[22] with the hopping as perturbation. In the cumulant expansion of the Anderson lattice[19] we employed the hybridization rather than the hopping as a perturbation, and the exact solution of the conduction electrons problem in the absence of hybridization was included in the zeroth-order Hamiltonian. It was then necessary to extend Metzner's derivation[22] to the Anderson lattice, and the same type of results he derived were also obtained for the Anderson lattice. As with the Feynman diagrams, one can rearrange all those that contribute to the exact $G_{ff,\sigma}(\mathbf{k},\omega_\nu)$ by defining an effective cumulant $M^{\text{eff}}_{2,\sigma}(\mathbf{k},\omega_\nu)$, that is given by all the diagrams of $G_{ff,\sigma}(\mathbf{k},\omega_\nu)$ that cannot be separated by cutting a single edge (usually called "proper"

TABLE I. The 16 eigenstates $|\nu,r\rangle$ of $\mathcal{H}$ are given as a function of the eigenstates in the absence of hybridization, together with their eigenvalues $\varepsilon_{\nu,r}=E_{\nu,r}-\nu\mu$, where $E_{\nu,r}$ is the energy of the state $|\nu,r\rangle$. To abbreviate we used $C\phi_{\pm}=\cos\phi_{\pm}$, $S\phi_{\pm}=\text{sen}\,\phi_{\pm}$, $C\psi_{\pm}=\cos\psi_{\pm}$ and $S\psi_{\pm}=\text{sen}\,\psi_{\pm}$.

$\|\nu,r\rangle$	Eigenstate	S_z	$\varepsilon_r=E_r-\nu_r\mu$
$\|0,1\rangle$	$\|-\frac{1}{2},0\rangle$	$-1/2$	$\varepsilon_1=E_-$
$\|0,2\rangle$	$\|+\frac{1}{2},0\rangle$	$+1/2$	$\varepsilon_2=E_+$
$\|1,3\rangle$	$C\phi_-\|-1,0\rangle-S\phi_-\|-\frac{1}{2},\downarrow\rangle$	-1	$\varepsilon_3=\varepsilon_{s-}+r_-$
$\|1,4\rangle$	$C\phi_+\|+1,0\rangle-S\phi_+\|+\frac{1}{2},\uparrow\rangle$	$+1$	$\varepsilon_4=\varepsilon_{s+}+r_+$
$\|1,5\rangle$	$S\phi_-\|-1,0\rangle+C\phi_-\|-\frac{1}{2},\downarrow\rangle$	-1	$\varepsilon_5=\varepsilon_{s-}-r_-$
$\|1,6\rangle$	$S\phi_+\|+1,0\rangle+C\phi_+\|+\frac{1}{2},\uparrow\rangle$	$+1$	$\varepsilon_6=\varepsilon_{s+}-r_+$
$\|1,7\rangle$	$\|-\frac{1}{2},\uparrow\rangle$	0	$\varepsilon_7=E_-+\varepsilon_+^0$
$\|1,8\rangle$	$\|+\frac{1}{2},\downarrow\rangle$	0	$\varepsilon_8=E_++\varepsilon_-^0$
$\|2,9\rangle$	$\|-1,\downarrow\rangle$	$-3/2$	$\varepsilon_9=\varepsilon_-+\varepsilon_-^0$
$\|2,10\rangle$	$\|+1,\uparrow\rangle$	$+3/2$	$\varepsilon_{10}=\varepsilon_++\varepsilon_+^0$
$\|2,11\rangle$	$C\psi_-\|-1,\uparrow\rangle-S\psi_-\|-\frac{1}{2},\uparrow\downarrow\rangle$	$-1/2$	$\varepsilon_{11}=\varepsilon_3+\varepsilon_+^0$
$\|2,12\rangle$	$C\psi_+\|+1,\downarrow\rangle-S\psi_+\|+\frac{1}{2},\uparrow\downarrow\rangle$	$+1/2$	$\varepsilon_{12}=\varepsilon_4+\varepsilon_-^0$
$\|2,13\rangle$	$S\psi_-\|-1,\uparrow\rangle+C\psi_-\|-\frac{1}{2},\uparrow\downarrow\rangle$	$-1/2$	$\varepsilon_{13}=\varepsilon_5+\varepsilon_+^0$
$\|2,14\rangle$	$S\psi_+\|+1,\downarrow\rangle+C\psi_+\|+\frac{1}{2},\uparrow\downarrow\rangle$	$+1/2$	$\varepsilon_{14}=\varepsilon_6+\varepsilon_-^0$
$\|3,15\rangle$	$\|-1,\uparrow\downarrow\rangle$	-1	$\varepsilon_{15}=\varepsilon_-+\varepsilon_2^0$
$\|3,16\rangle$	$\|+1,\uparrow\downarrow\rangle$	$+1$	$\varepsilon_{16}=\varepsilon_++\varepsilon_2^0$

or "irreducible" diagrams). The exact one-particle GFs of the Anderson lattice[13,23] were then obtained by introducing the $M_{2,\sigma}^{\text{eff}}(\mathbf{k},\omega_\nu)$ in the cumulant expansion, and the model employed in those works was sufficiently general so that their results could be easily extended to the Hamiltonian in Eq. (2) in the present work.

By analytical continuation one then obtains the formal expressions of the exact one-particle GFs of our model

$$G_{ff,\sigma}(\mathbf{k},z)=\frac{M_{2,\sigma}^{\text{eff}}(\mathbf{k},z)}{1-|V(\mathbf{k})|^2G_{c,\sigma}^{o}(\mathbf{k},z)M_{2,\sigma}^{\text{eff}}(\mathbf{k},z)},\tag{9}$$

and

$$G_{cc,\sigma}(\mathbf{k},z)=\frac{-1}{z-\varepsilon_{\mathbf{k}\boldsymbol{\sigma}}+|V(\mathbf{k})|^2M_{2,\sigma}^{\text{eff}}(\mathbf{k},z)},\tag{10}$$

where $G_{c,\sigma}^{o}(\mathbf{k},z)=-1/(z-\varepsilon_{\mathbf{k}\boldsymbol{\sigma}})$ is the free c-electron propagator.

The calculation of $M_{2,\sigma}^{\text{eff}}(\mathbf{k},\omega_\nu)$ is as difficult as that of $G_{ff,\sigma}(\mathbf{k},\omega_\nu)$, and it is then convenient to use an approximation: We shall replace $M_{2,\sigma}^{\text{eff}}(\mathbf{k},\omega_\nu)$ by the corresponding quantity $M_{2,\sigma}^{\text{at}}(\omega_\nu)$ of an exactly soluble Hamiltonian, namely, the one describing the atomic limit of the same model. Although the hopping is neglected in this system, described by the Hamiltonian of Eqs. (2) with $E_{\mathbf{k},\sigma}=E_{0,\sigma}$ and with a local hybridization $V(\mathbf{k})=V$, the $M_{2,\sigma}^{\text{at}}(\omega_\nu)$ implicitly contains all the higher order cumulants that appear in the exact quantity. In the case of the Anderson lattice, the atomic limit contains the basic physics of the formation of the singlet ground state and of the appearance of the Kondo peak,[24,25] and we expect that it would provide an adequate description of the present model. Because of its atomic character, the approximate effective cumulant $M_{2,\sigma}^{\text{at}}(\omega_\nu)$ thus obtained is independent of $\mathbf{k}$, and can be calculated exactly as discussed below.

With the approximations introduced above and employing the Wannier representation for the c-electron operators the whole system becomes a collection of local systems, described by a Hamiltonian $\Sigma_j H_j$, where H_j is the local Hamiltonian at site j. This H_j can be solved exactly

$$H_j|j,\nu,r\rangle=E_{\nu,r}|j,\nu,r\rangle,\tag{11}$$

where $|j,\nu,r\rangle$ is the eigenstate at site j with energy $E_{\nu,r}$, that is characterized by r and its number ν of electrons. Because of the translational invariance we shall drop the site index j when it is not necessary, and we shall also use the quantities $\varepsilon_{\nu,r}=E_{\nu,r}-\nu\mu$, more adequately for the $\mathcal{H}$ in Eq. (4) than the $E_{\nu,r}$ (for convenience we use $\nu_{\pm\frac{1}{2}}=0$ and $\nu_{\pm1}=1$). In Table I (cf. notation in Appendix A) we give the properties of the $|\nu,r\rangle$ states: The number r that identifies the state, the z component of spin S_z, and the quantities $\varepsilon_{\nu,r}=E_{\nu,r}-\nu\mu$.

It is now straightforward to express the Fourier transform $G_{ff,\sigma}^{\text{at}}(\omega_s)$ of the f-electron GF in the atomic limit

$$G_{ff,\sigma}^{\text{at}}(\omega_s)=-e^{\beta\Omega}\sum_{\nu,r,r'}\frac{\exp(-\beta\varepsilon_{\nu,r})+\exp(-\beta\varepsilon_{\nu-1,r'})}{i\omega_s+\varepsilon_{\nu-1,r'}-\varepsilon_{\nu,r}}\times|\langle\nu-1,r'|X_{\sigma,s=2\sigma}|\nu,r\rangle|^2,\tag{12}$$

where $\Omega=-kT\ln\Sigma\exp(-\beta\epsilon_{\nu,r})$ is the grand canonical potential.[26] The equivalent equations for the c electrons are obtained by just replacing $|\langle\nu-1,r'|X_{\sigma,s=2\sigma}|\nu,r\rangle|^2$ in Eq. (12) by $|\langle\nu-1,r'|C_{j,\sigma}|\nu,r\rangle|^2$.

The f-electron GF can be written in the form

$$G^{\mathrm{at}}_{ff,\sigma}(\omega_s) = -\exp(\beta\Omega)\sum_{j=1}^{8}\frac{m_j}{i\omega_s - u_j}, \tag{13}$$

and the poles u_i and residues m_i of $G^{\mathrm{at}}_{ff,\sigma}(\omega_s)$ are all real [cf. Eq. (12)]. There are only eight different u_j for the f-electron GF, because different transitions have the same energy and the residues of some transitions are zero, and by analytical continuation one obtains $G^{\mathrm{at}}_{ff,\sigma}(z)$, but there are more transitions for the $G^{\mathrm{at}}_{cc,\sigma}(z)$.

The approximation employed in the present work consists in substituting $M^{\mathrm{eff}}_{2,\sigma}(z)$ in Eq. (9) by the approximate $M^{\mathrm{at}}_{2,\sigma}(z)$, derived from the exact $G^{\mathrm{at}}_{ff,\sigma}(z)$ by solving for $M^{\mathrm{at}}_{2,\sigma}(z)$ in the equation that is the atomic equivalent of Eq. (9). One then obtains

$$M^{\mathrm{at}}_{2,\sigma}(z) = \frac{(z - E^a_0 + \mu)G^{\mathrm{at}}_{ff,\sigma}(z)}{(z - E^a_{0,\sigma} + \mu) - |V|^2 G^{\mathrm{at}}_{ff,\sigma}(z)}, \tag{14}$$

and from the point of view of the cumulant expansion, it contains all the irreducible diagrams that contribute to the exact $M^{\mathrm{eff}}_{2,\sigma}(\omega_s)$. It should be emphasized that these diagrams contain loops of any size, because there is no excluded site in this expansion, but all the local vertices correspond to the same site, although they appear as different vertices in each diagram. When a local hybridization is used [i.e., $V(\mathbf{k})=V$], the only difference between the exact and approximate quantities is that different energies $E_{\mathbf{k},\sigma}$ appear in the c-electron propagators of the effective cumulant $M^{\mathrm{eff}}_{2,\sigma}(\omega_s)$, while these energies are all equal to $E^a_{0,\sigma}$ in $M^{at}_{2,\sigma}(\omega_s)$. Although $M^{at}_{2,\sigma}(\omega_s)$ is for that reason only an approximation, it contains all the diagrams that should be present, and one would expect that the corresponding GF would have fairly realistic features.

One still has to decide what value of $E^a_{0,\sigma}$ should be taken. As the most important region of the conduction electrons is the Fermi energy, we shall use $E^a_{0,\sigma}=\mu-\delta E_0$, leaving the freedom of small changes δE_0 to adjust the results to particular situations, but fixing its value for a given system when μ has to change to keep the total number of electrons N_t fixed, as for example when changing the temperature T.

Another important point is that concentrating all the conduction electrons at $E^a_{0,\sigma}$ would overestimate their contribution to the effective cumulant, and we shall then reduce the hybridization by a coefficient that gives the fraction of c electrons that contribute most. We consider that this is of the order of $V\varrho^0$, where ϱ^0 is the density of states of the free c electrons per site and per spin, and to be more definite we chose $\pi V\varrho^0$, so the effective hybridization constant V_a coincides with the usual "mixing strength" $\Delta=\pi V^2\varrho^0$. This is essentially the same choice made by Alascio *et al.*[27] in their localized description of valence fluctuations. Note that V_a is used only in the calculation of $M^{\mathrm{at}}_{2,\sigma}(z)$, and that the full value must be substituted in the V that appears explicitly in Eq. (9), because the whole band of conduction energies is used in $G^o_{c,\sigma}(\vec{k},z)=-1/(z-\varepsilon_{\mathbf{k}\sigma})$.

B. Transport properties

Two-particle GF should be used in the well-known Kubo formula,[28,29] that relates the dynamic conductivity $\sigma(\omega,T)$ to the current current correlations. To simplify the calculations for the Anderson lattice, Schweitzer and Czycholl[30] employed the expression of the conductivity for dimension $d=\infty$ as an approximation of the static conductivity for $d=3$. Only one-particle GFs are then necessary to obtain $\sigma(\omega,T)$ in that limit, because the vertex corrections cancel out,[31] and we shall use here the same approximation. As the hybridization is a hopping of electrons between two different bands, it contributes to the current operator,[32] but this contribution cancels out in our model because we employ a local hybridization $V_{j,\mathbf{k},\sigma}=V_{j,\sigma}$. The expression obtained contains explicit sums over $\mathbf{k}$, but it is possible to make a further simplification by considering nearest-neighbor hopping in a simple cubic lattice,[33–35] and the sums over $\mathbf{k}$ can be transformed[36] in integrals over the free conduction electron energy $\varepsilon(\mathbf{k})$. This transformation is possible because in our method the $G_{cc,\sigma}(\mathbf{k},\omega)$ only depends on $\mathbf{k}$ through the $\varepsilon(\mathbf{k})=\varepsilon$, as both $M^{\mathrm{at}}_{2,\sigma}(z)$ and $V_{j,\mathbf{k},\sigma}=V_{j,\sigma}$ are $\mathbf{k}$ independent. We then obtain for the dynamic conductivity for each spin component

$$\sigma_\sigma(\omega,T) = C_0\frac{1}{\omega}\int_{-\infty}^{\infty} d\omega'[f_T(\omega') - f_T(\omega'+\omega)]L_\sigma(\omega,\omega'), \tag{15}$$

where

$$L_\sigma(\omega,\omega') = \int_{-\infty}^{\infty} d\varepsilon\ \rho_{c,\sigma}(\omega';\varepsilon)\rho_{c,\sigma}(\omega'+\omega;\varepsilon)\varrho^0_\sigma(\varepsilon), \tag{16}$$

$$\rho_{c,\sigma}(\omega;\varepsilon) = \frac{1}{\pi}\lim_{\eta\to 0}\mathrm{Im}\{G_{cc,\sigma}(\mathbf{k},\omega+i|\eta|)\}, \tag{17}$$

and $f_T(\omega)$ is the Fermi function. The static conductivity for each spin component is then given by

$$\sigma_\sigma(T) = C_0\int_{-\infty}^{\infty} d\omega\left(-\frac{df_T(\omega)}{d\omega}\right)L_\sigma(\omega), \tag{18}$$

where

$$L_\sigma(\omega) = \int_{-\infty}^{\infty} d\varepsilon[\rho_{c,\sigma}(\omega;\varepsilon)]^2\varrho^0_\sigma(\varepsilon). \tag{19}$$

The constant

$$C_0 = \pi\frac{e^2}{\hbar}\frac{2}{a}\frac{2}{d}t^2, \tag{20}$$

where $a=9.89$ Å is the lattice parameter[4] of $Tl_2Mn_2O_7$, which has two sites per unit cell. We shall generally use a rectangular band with $-W\leq\varepsilon(\mathbf{k})\leq W$, and we set $t=W/2d$ to estimate the hopping parameter t of the hypercubic lattice, and use $d=3$.

Employing Ref. 30 we obtain the expression for the thermopower $S(T)$

$$S(T) = \frac{\sum_{\sigma} \int_{-\infty}^{\infty} d\omega\ \omega(-df_T(\omega)/d\omega) L_{\sigma}(\omega)}{eT \sum_{\sigma} \int_{-\infty}^{\infty} d\omega (-df_T(\omega)/d\omega) L_{\sigma}(\omega)}. \quad (21)$$

C. Magnetization of the system

As the system consists of two independent subsystems (spin up and spin down), we could attribute arbitrary probabilities $P(1-P)$ of finding local electrons with spin up (with spin down), and calculate the corresponding properties of the system. Following the work of Ventura and Alascio, we shall estimate the probability P from the system magnetization that we calculated employing the Weiss molecular field approximation

$$\frac{M}{M_{\text{sat}}} = \tanh\left\{ \frac{\tilde{\mu}\, B}{k_B T} + \frac{T_C M}{T\, M_{\text{sat}}} \right\}. \quad (22)$$

Here $\tilde{\mu}$ is the local magnetic moment, B the magnetic field, T_C the Curie temperature and M_{sat} the saturation magnetization. Following those authors we use $\tilde{\mu}=3\mu_B$, as intermediate between the 3.87 μ_B local moment of the Mn^{4+} and the 2.83 μ_B corresponding to the Mn^{5+}.[47]

To calculate the probability P we then employ

$$M = [P - (1-P)]\tilde{\mu}, \quad (23)$$

and proceed to calculate the system properties as a function of T for different values of the total number n of electrons per site. Employing our approximate GF it is possible to calculate n for each value of P and T, and it is then necessary to find the chemical potential μ that gives the required number of electrons per site.

We should point out that we are not proposing a model to explain the magnetization of the system, but we are only using the Weiss molecular field as an algorithm that approximately gives the magnetization of the system, starting from the experimental saturation magnetization M_{sat} and the Curie temperature T_C.

III. CALCULATION OF THE TRANSPORT PROPERTIES

We shall consider the stoichiometric $Tl_2Mn_2O_7$ compound, and we shall then fix the total number of electrons per site as $n=1$. To keep this value constant, it might be necessary to change the chemical potential μ with the temperature T, and we shall employ the approximate GFs $G^{\text{at}}_{ff,\sigma}(z)$ and $G^{\text{at}}_{cc,\sigma}(z)$ to calculate the number n at each T and then solve numerically the equation $n=1$.

We shall use a rectangular band centered at the energy origin and with a half width $W=6$ eV, and take the energies for the spin 1/2 and 1 in the presence of the field B as $E_{\sigma} = 2\sigma\ \mu_B B$ and $E_s = E_s^0 + s\ 2\mu_B B$, with $E_s^0 = -5.5$ eV, so that the spin 1 (corresponding to Mn^{4+}) has the lowest energy of the local states at $B=0$.

It seems clear that the basic scattering mechanism in our calculation of $\sigma(T)$ is the hybridization, because the otherwise free conduction electrons are scattered by the localized f electrons through this interaction, and it seems clear that the resistivity at low temperatures depends sensitively on the value of V. This quantity also determines the position of the peak of the dynamic conductivity that is close to 2 eV at 295 K, and to try and adjust the two different properties we have employed a temperature dependent hybridization V, using values that decrease from 2.5 to 1.8 eV as T increases to 300 K.

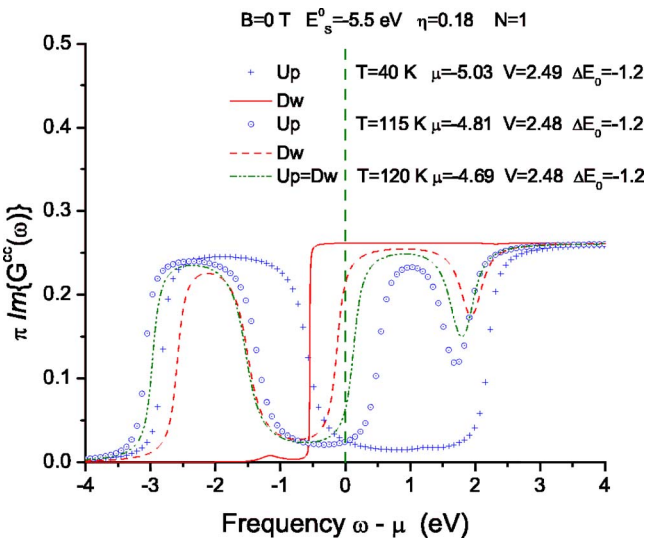

FIG. 1. (Color online) Local spectral density of the conduction electrons $\rho_{c,\sigma}(\omega)$ at $T=40$ K, $T=115$ K, and $T=T_C=120$ K, for the system parameters indicated in the figure. We employ a T dependent V and ΔE_0, and their values together with μ are shown for each curve.

We have also employed a value of $\Delta E_0 = E_0^a - \mu$ that changes from -1.2 eV to -0.9 eV in the same temperature range, because it gives a better overall agreement with the experimental results.

To alleviate somehow the use of a zeroth width conduction band in the calculation of the effective cumulant we have added an extra imaginary part $\eta_a=0.18$ eV to the complex variable z, and this procedure is further discussed in Appendix B.

A. Local spectral density of states

A very useful quantity is the local spectral density of the conduction electrons, namely,

$$\rho_{c,\sigma}(\omega) = \frac{1}{\pi} \lim_{\eta \to 0} \text{Im} \left\{ \frac{1}{N_s} \sum_{\mathbf{k}} G_{cc,\sigma}(\mathbf{k}, \omega + i|\eta|) \right\} \quad (24)$$

because it illuminates the dependence with T of the static conductivity. In Fig. 1 we plot $\rho_{c,\sigma}(\omega)$ at two temperatures below the critical temperature $T_C=120$ K and also at T_C, for parameters that give a fair description of the properties we study.

At $T=40$ K the $\rho_{c,\sigma}(\omega)$ are different for the two spin components. The magnetization is practically saturated and all the local spins point in the same direction, say up. The con-

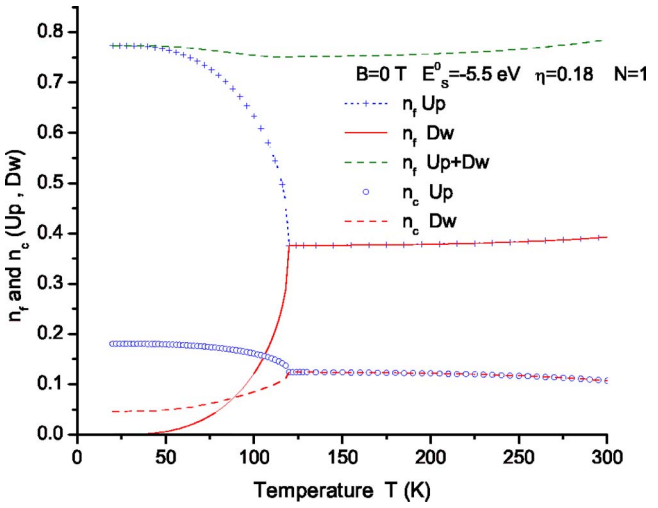

FIG. 2. (Color online) Number of local and conduction electrons per site for spin up and spin down, as well as the total number of local electrons per site, as a function of T. The system parameters are indicated in the figure.

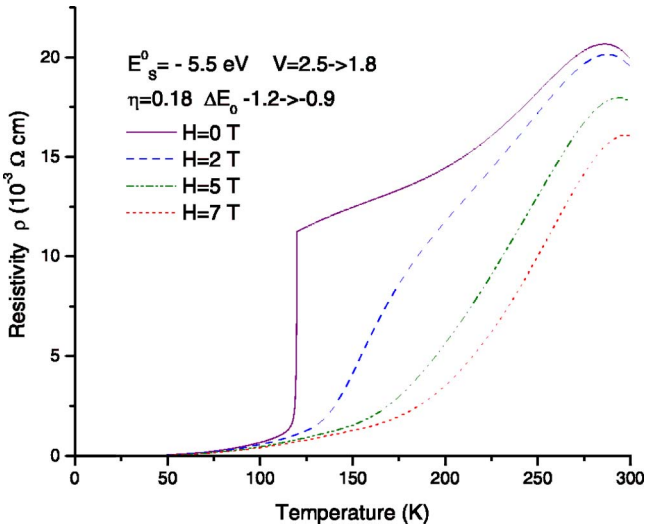

FIG. 3. (Color online) Resistivity as a function of T for several magnetic fields, and for the system parameters indicated in the figure.

duction electrons with spin up hybridize with the local spins, and in Fig. 1 it is shown that a large gap is created with μ inside, so there is practically no conductivity by these electrons. As there are practically no local electrons with spin down, the conduction electrons do not have electrons to hybridize with, and there is no gap. The chemical potential μ is near the bottom of the band, and the spin down electrons contribute strongly to the conductivity giving a vanishing resistivity as is shown in Fig. 3.

We also plot $\rho_{c,\sigma}(\omega)$ at $T=115$ K, i.e., just below T_C; there is now a large number of local electrons with spin down, and the two $\rho_{c,\sigma}(\omega)$ are very similar for the two spins. The two spins have the same spectral density at T_C, and the curves at higher T are similar to that at T_C, but with a smaller gap because we employ a hybridization that decreases with T. The μ is inside the gap in all the curves above T_C, and the resistivity increases abruptly at T_C, as shown in Fig. 3.

From Hall measurements it has been estimated[37] that the number of carriers at low T is at most 0.005, and to discuss this problem we have calculated the number of up ($n_{c,\mathrm{up}}$) and down ($n_{c,\mathrm{dw}}$) conduction electrons per site and the corresponding ($n_{f,\mathrm{up}}$) and ($n_{f,\mathrm{dw}}$) for the local electrons, by integrating the corresponding spectral densities $\rho_{c,\sigma}(\omega)$ and $\rho_{f,\sigma}(\omega)$ over ω. We plot these quantities as a function of T in Fig. 2, as well as the total number of local electrons $n_f = n_{f,\mathrm{up}} + n_{f,\mathrm{dw}}$, that is fairly independent of T and close to $n_f = 0.77$, so that the total number of c electrons resulting from the hybridization with the f electrons is close to 0.23. This value seems to contradict the Hall measurement value, but from Fig. 1 we should notice that all the conduction electrons with spin up are filling up the lower band at low T, and they would not contribute to the conductivity nor to the number of carriers measured by the Hall effect. In Fig. 2 we see that $n_{c,\mathrm{dw}}=0.04$ at low T, and although this value is larger than the experimental one, it has the qualitative behavior of the measured quantity, namely, it is a rather small number. We have not tried to adjust explicitly the low carrier concentration, so that our results only describe the experimental results in a semiquantitative way.

Looking at the T dependence of $\rho_{c,\sigma}(\omega)$ in Fig. 1 we see that the lower band with down spins grows with T, and becomes identical to the band with spins up at T_C, so that the number of carriers decreases with T. The increase in the concentration of down spin with T in Fig. 2 is then due to the increase of the lower band, that does not contribute to the number of carriers measured in the Hall effect. This corresponds from Fig. 1 to a decrease in the number of carriers with increasing T, and this has been observed experimentally as shown in Fig. 2 of Ref. 9.

We have shown in Fig. 2 that the number n_f of local electrons is fairly independent of T, a fact that agrees with the measurements of x-ray absorption spectroscopy (XAS) in $Tl_2Mn_2O_7$,[38] which indicate that the Mn valence is fairly close to 4. Two facts point out to the independence of this quantity with temperature. First, the XAFS indicates that the local structure coincides with the average one in $Tl_2Mn_2O_7$ and that there is no disorder in the same structures of this compound, differently from the disorder in the MnO_6 octahedra of the manganites, that is caused by Jahn-Teller distortions. Second, the Mn-O and Tl-O bonds in $Tl_2Mn_2O_7$ show normal Debye-like dependence, with no change in ordering at T_c, in contrast with the behavior of the $La_{0.75}Ca_{0.25}MnO_3$ manganite.[38]

Subramanian *et al.*[37] conclude from the properties of $Tl_2Mn_2O_7$ that some of the Mn^{4+} electrons go into the Tl band, so that the compound corresponds to $Tl^{3+}_{2-x}-Tl^{2+}_x Mn^{4+}_{2-x} Mn^{5+}_x O_7$, in agreement with the model of Ventura and Alascio.[12]

B. Static resistivity and the magnetoresistance

We employ Eq. (18) to calculate the conductivity for each spin component, and we sum the two contributions to obtain the total conductivity. In Fig. 3 we plot the resulting resistiv-

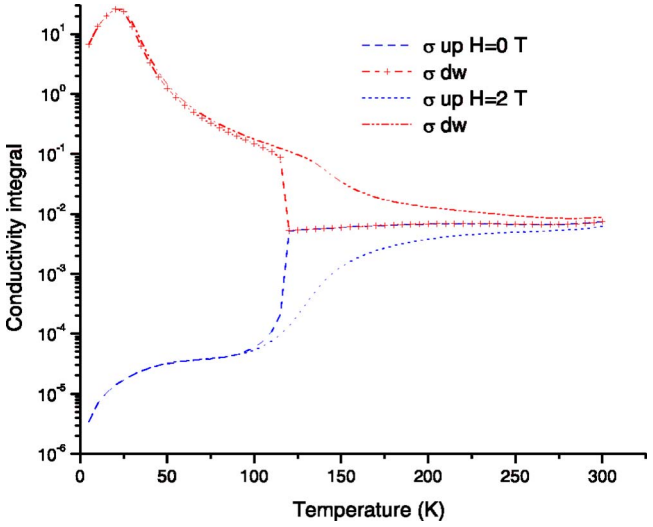

FIG. 4. (Color online) Values proportional to $\sigma_\sigma(T)$ for up and down electrons at $H=0$ T and $H=2$ T, for the same parameters given in Fig. 3

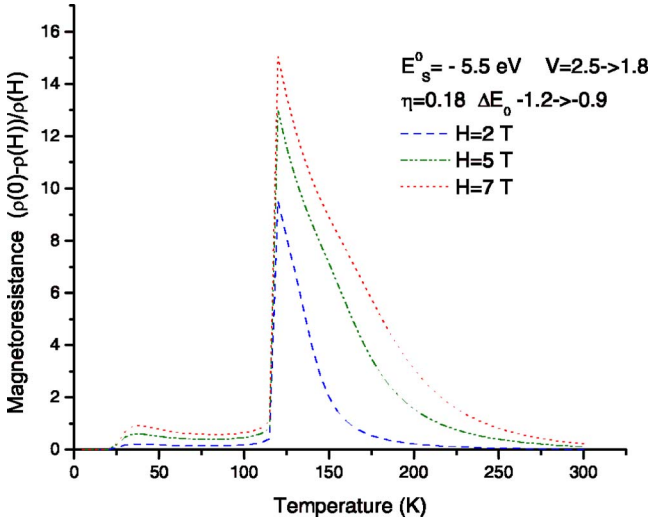

FIG. 5. (Color online) Magnetoresistance as a function of T for several magnetic fields, and for the system parameters indicated in the figure.

ity as a function of T for the following magnetic fields: $B=0$, 2, 5, and 7 T, and the remaining system parameters are given in the figure. The values we calculated are of the same order of those reported by Shimakawa *et al.*,[14] and there is a sharp but continuous increase in the resistance at the critical temperature T_C; the increase becomes more gradual at higher magnetic fields.

In Fig. 4 we plot quantities proportional to $\sigma_\sigma(T)$ for the up and down electrons at both $H=0$ T and $H=2$ T. Is is clear that the spin up electrons have a very small conductivity up to values of T close to T_C, in agreement with our interpretation in the previous section that they do not provide carriers to the system. The small increase approaching to T_C is due to the shift in the chemical potential μ, as well as to the change in shape of the spectral density, that result in a few carriers with spin up appearing in the upper band.

From the resistivity at different magnetic fields we calculated the negative magnetoresistance $[\rho(B=0)-\rho(B)]/\rho(B)$, plotted in Fig. 5. The value of the maximum near T_C is close to that observed by Cheong *et al.*,[8] but the rise before the maximum, like that of the resistance, is much steeper in our calculation. The origin of this sudden rise is the rather fast decrease in the magnetization at zero magnetic field, that is directly related to the probability P and the corresponding decrease in the number of carriers with spin down, which is apparent in Fig. 1. We believe that the change in resistivity would be smoother if we used a density of states that is not so sharp as the rectangular one, but we have not tried this modification.

C. Optical conductivity

We have employed Eq. (15) to calculate the optical conductivity $\sigma(\omega,T)$ as the sum of the contribution $\sigma_\sigma(\omega,T)$ of the two spin components. In the measurements of the optical conductivity of Okamura *et al.*[15] one observes a strong peak close to $\omega=2$ eV at $T=295$ K. This type of measurement is expected to depend on the value of the direct gap, which is affected by the hybridization constant V. The static resistivity, on the other hand, depends on the indirect gap, and the scattering mechanism at low temperatures depends also on the hybridization, as discussed before. We have then employed a temperature dependent value of V to adjust these two quantities, and we used $V\simeq 1.85$ eV at $T=295$ K. In Fig. 6 we plot the the optical conductivity $\sigma(\omega,T)$ at $T=295$ K, and we obtain a peak at the correct frequency. There are several smaller peaks at lower frequencies that have been assigned to optical phonons.[15]

At low T the two spin components make different contributions to $\sigma(\omega,T)$, as shown in Fig. 7.

The component with spin down corresponds to a metal, and the corresponding $\sigma(\omega,T)$ describes the Drude peak of this metal, and the figure shows that the metallic components are limited to below 0.5 eV, as measured by Okamura *et al.*[15]

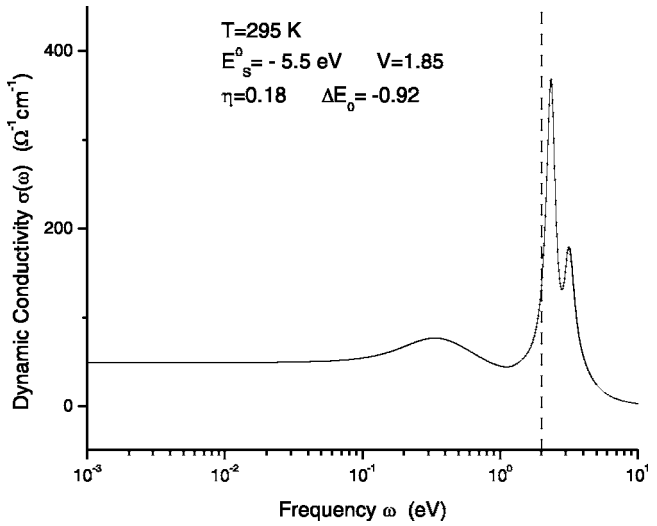

FIG. 6. Optical conductivity for the system parameters indicated in the figure.

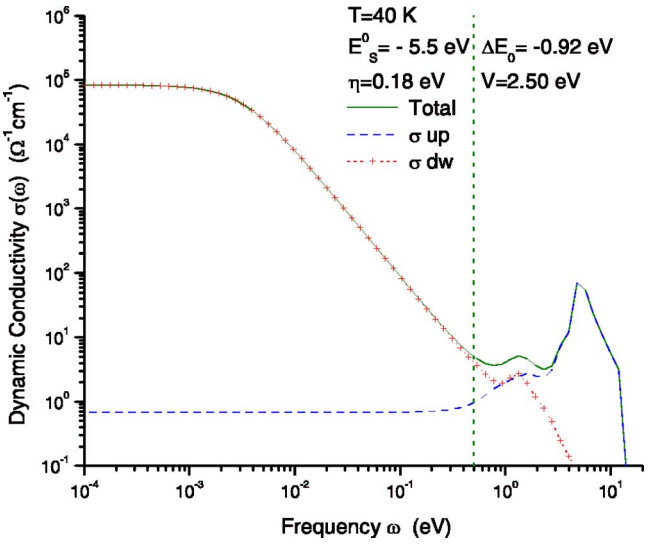

FIG. 7. (Color online) Contribution of the two spin components to the optical conductivity at $T=40$ K for the system parameters indicated in the figure. The vertical line is located at 0.5 eV.

Although the spectral density in Fig. 1 does not give the direct gap, it is consistent with Fig. 7. The spin up component in Fig. 1 corresponds to a semiconductor, and in Fig. 7 it shows a very small $\sigma(\omega,T)$ at low frequencies, that starts to increase at $\omega\sim 3$ eV. The different contribution of the two spin components can also be understood by considering the sum rules[23,39,40] of the two spin components of $\sigma_\sigma(\omega,T)$ as two separate contributions, but we have not done a numerical analysis of this interpretation. The two components give identical contributions to $\sigma_\sigma(\omega,T)$ above T_C, because the two bands are identical when the magnetization becomes zero.

In Fig. 8 we plot the optical conductivity for several temperatures. At low frequencies one can see how the maximum of the Drude peak at $\omega=0$ decreases and its width increases when T increases.

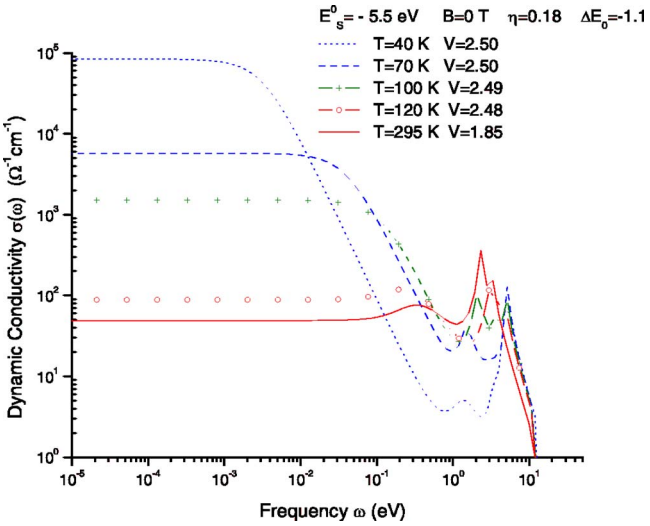

FIG. 8. (Color online) Optical conductivity at low frequencies for several temperatures.The values of $\sigma(\omega,T)$ when $\omega\rightarrow 0$ give the temperature dependence of the Drude peak

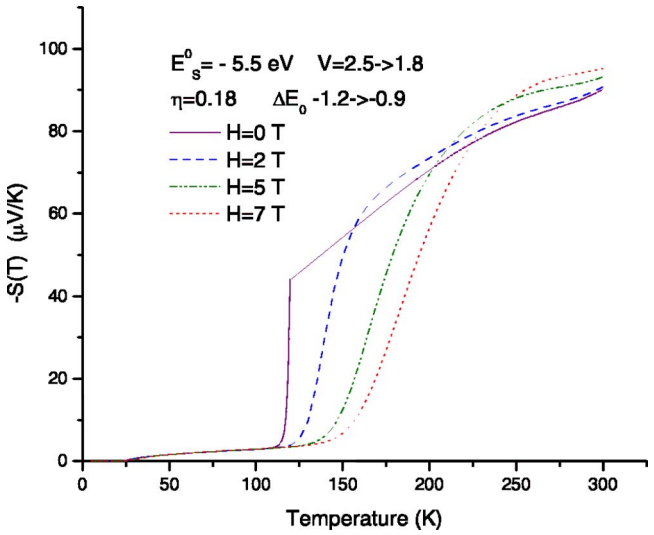

FIG. 9. (Color online) Thermopower for the system parameters indicated in the figure.

D. Thermopower and the magnetothermopower

We have employed Eq. (21) to calculate the thermopower $S(H,T)$ of $Tl_2Mn_2O_7$ within the model of Ventura and Alascio,[12] and in Fig. 9 we show the temperature dependence for several magnetic fields.

The plot agrees qualitatively with the experimental results of Imai *et al.*[9] and at $H=0$ T it is approximately linear in T just below and above T_C, but with different slopes. We employed Eq. (21) to calculate $S(H,T)$, because the model is composed of two independent subsystems. It is then straightforward to calculate the magnetothermopower, defined by $\Delta S(H)=S(H)-S(0)$, and in Fig. 10 we plot our results, which show a semiquantitative agreement with those in Ref. 9: The magnitude of $\Delta S(H)$ is of the same order, but the increase at T_C is more abrupt than the one measured experimentally.

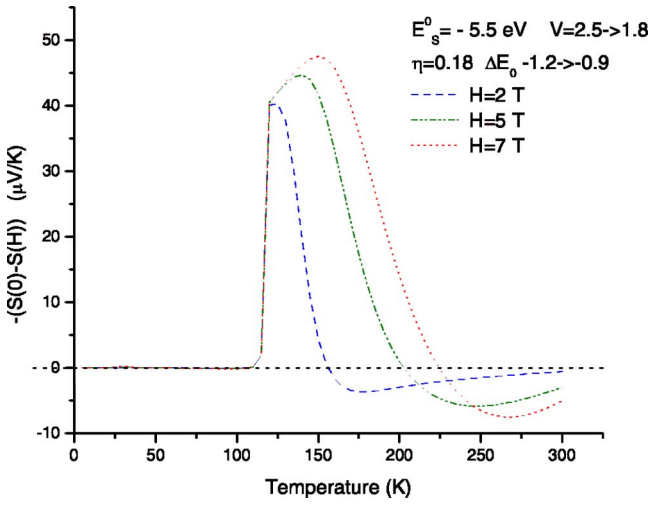

FIG. 10. (Color online) Magnetothermopower for the system parameters indicated in the figure.

IV. MAGNETIC POLARONS

We have obtained approximate GF for the model employed by Ventura and Alascio[12] to describe the resistivity and CMR of $Tl_2Mn_2O_7$, and it would be interesting to compare its physical properties to those of an alternative model that has been applied,[41–44] at temperatures above T_C. In this last approach, a gas of electrons coupled with magnetic fluctuations is considered at temperatures close to and above the magnetic transition temperature T_C. At low electronic densities, each carrier can polarize a small ferromagnetic cluster of local spins, and be self-trapped by their magnetic moments: this arrangement is a free magnetic polaron (FMP), and the cluster size increases when we approach T_C. When the FMP begin to overlap, the carriers can move freely and the transport mechanism is then described by their scattering with the magnetic fluctuations of the localized moments. Majundar and Littlewood[41] studied this itinerant regime using an extension of the work of Fisher and Langer,[45] and they also estimated the size and energy of the FMP. Employing the ionization energy of the carrier electron in the FMP to the conduction band as an activation energy, they obtained the resistivity of the FMP, and they concluded that the magnetoresistance is large in both the bound and itinerant regimes. A Monte Carlo calculation of the FMP in two dimensions was also presented in Ref. 43, indicating that they are considerably more weakly bound than shown in the mean field picture employed in Ref. 41. An alternative mechanism that does not requires activation was proposed by Wegener and Littlewood in Ref. 44. It considers that when a fluctuation of the magnetic moments neighboring the FMP makes them parallel to those of the polaron, the carrier can tunnel to that region without any activation energy, and the whole process corresponds to a displacement of the FMP. This is a diffusive process of the FMP, and estimating the corresponding diffusion constant D they calculated the resistivity ρ by employing Einstein's relation $\rho=k_BT/(ne^2D)$, where n is the number density of the polarons.

The model Hamiltonian employed to study the FMP is[44]

$$H=-t\sum_{\langle i,j\rangle\sigma} c^{\dagger}_{i,\sigma}c_{j,\sigma}-J'\sum_{i}\vec{\sigma}_i\cdot\vec{S}_i-J\sum_{\langle i,j\rangle}\vec{S}_i\cdot\vec{S}_j, \qquad (25)$$

where the first term describes the conduction band, the second represents the "*s-d*" interaction between all the localized spins $\vec{S}_i$ and the corresponding spins $\vec{\sigma}_i$ of the conduction electron in the Wannier representation, and the third term describes the super exchange interaction between the localized spins.

The first term is essentially the same as the third term of our model Hamiltonian in Eq. (2), while the remaining terms have different physical interpretations.

The first two terms in Eq. (2) describe the two magnetic configurations with spin $S=1/2$ and $S=1$ of each local state, and by discarding the $S=1$ local state with $S_z=0$ at each site, the system can be described by two independent systems with spin up and spin down, respectively, because the hybridization [fourth term in Eq. (2)] conserves the spin direction. There is no equivalent term in Eq. (25), because there is no charge fluctuation in the local moments, and their corresponding ground energy is not included explicitly in the Hamiltonian.

The main source of resistivity in Eq. (25) is the second term, while in our model it is the hybridization, described by the fourth term in Eq. (2). Although in the Anderson model the hybridization gives a "*s-d*" interaction through the Schrieffer–Wolf transformation,[25] that interaction is absent in our model because there is no state with $S_z=0$ that is responsible for the spin-flip transitions.

The third term in Eq. (25) is considered implicitly in our model, because we assume that there is a temperature dependent magnetization M, which we estimate employing the Weiss molecular field approximation, and we use this value and Eq. (23) to obtain the probability $P(1-P)$ of finding the spin up (spin down) subsystem. In the Weiss approximation there are no fluctuations of the local moments, and it is then clear that to include something equivalent to the FMP in our model it would be necessary to treat the superexchange with a method beyond the mean field Weiss approximation.

In our model, the change of conductivity at low T depends mainly on the change of P: When $P=1$ there are no local spins down, and the carriers of the same spin cannot hybridize. The Fermi energy is well inside the band for the parameters employed (cf. Fig. 1), and these electrons would appreciably contribute to the conductivity. The states with spin up are strongly hybridized, and their Fermi energy is just in the hybridization gap (cf. Fig. 1), so that the material is a half-metal, with all the conductivity provided by the spin down electrons. When T increases, so does the number of local spins down, and the hybridized band deforms at the same time that its occupation decreases, tending to $(1-P)=0.5$ at T_C. The hybridization also affects the resistivity by acting as a scattering potential, as discussed in Appendix B.

In our method we obtain approximate GF, and with them it is possible to derive several physical properties at all T, while only the resistivity at T well above T_C can be obtained, through the use of Einstein's relation, in the method that employs the FMP.

V. CONCLUSIONS

Assuming that the system is stoichiometric we have calculated the resistivity, optical conductivity, and thermopower as a function of temperature and magnetic field of the model of $Tl_2Mn_2O_7$ introduced by Ventura and Alascio.[12] Differently from other studies, we have calculated these transport properties employing Kubo's formula, which is directly related to the electronic GFs. To derive these GFs we introduced Hubbard operators to describe the model, and used a treatment previously employed to study FeSi.[13,23] Employing the dependence of resistivity and thermopower with magnetic field we have also calculated the magnetoresistance and the magneto thermopower.

We obtain a semiquantitative agreement with the experimental results by an adequate choice of the system parameters, and we can conclude that the model gives a fair description of all the calculated properties.

ACKNOWLEDGMENTS

The authors would like to acknowledge financial support from the following agencies: FAPESP and CNPq. They are grateful to B. Alascio and C. I. Ventura for suggesting this study and for several interesting discussions, and also to C. H. Booth for pointing out the results of Ref. 38.

APPENDIX A: ATOMIC EIGENSTATES

In Table I we give the atomic eigenstates $|j,\nu,r\rangle$ of H_j [cf. Eq. (11)] as a function of the eigenstates for $V=0$. To abbreviate we use $E_{\pm}=E_{\pm 1/2}$, $\varepsilon_{\pm}=E_{\pm 1}-\mu$, $\varepsilon_{\pm}^0=E_{0,\pm}^a-\mu$, and $\varepsilon_2^0=\varepsilon_+^0+\varepsilon_-^0$ as well as the following energy expressions that appear often in the formulas:

$$\varepsilon_{m\pm}=(\varepsilon_{\pm}-E_{\pm}-\varepsilon_{\pm}^0)/2,$$

$$\varepsilon_{s\pm}=(\varepsilon_{\pm}+E_{\pm}+\varepsilon_{\pm}^0)/2,$$

$$r_{\pm}=\sqrt{(\varepsilon_{m\pm})^2+|V|^2}.$$

The coefficients of the eigenfunctions in Table I are obtained from

$$tg\,\phi_{\pm}=\pm tg\ \psi_{\pm}=\frac{V^*}{\varepsilon_{m\pm}+r_{\pm}},$$

and we conventionally use $\cos\phi_{\pm}>0$ and $\cos\psi_{\pm}>0$ to specify the sign of the eigenfunctions.

APPENDIX B: DEPENDENCE OF THE RESISTIVITY WITH THE EFFECTIVE CUMULANT

As discussed in Sec. II B, the static conductivity for each spin component is given by Eq. (18), where the spectral density in Eq. (17)

$$\rho_{c,\sigma}(\omega;\varepsilon)=\frac{1}{\pi}\lim_{\eta\to 0}\mathrm{Im}\{G_{cc,\sigma}(\mathbf{k},\omega+i|\eta|)\}$$

is employed. If in Eq. (10) we abbreviate $G_{cc,\sigma}(\mathbf{k},z)=-[a-\varepsilon(\mathbf{k})+i\,b]^{-1}$, with real a and b (functions of ω) defined by $a+i\,b=z+|V|^2\,M_{2,\sigma}^{\mathrm{at}}(z)$, we find that when $b\to 0$ then $L(\omega)\sim \mathrm{O}|1/b|$ if ω is outside the gap and $S(\omega)\sim \mathrm{O}|b^2|$ if ω is inside. This property can give rather different low T limits of $\sigma(T)$, because the integrand in Eq. (18) only contributes in an interval of $\mathrm{O}|T|$ around the Fermi energy $\omega=0$ (our frequency variables are given with respect to μ). When $\omega=0$ is inside the gap and $\mathrm{Im}\,M_{2,\sigma}^{\mathrm{at}}(0)\sim 0$ we then have a very small $\sigma(0)$, while $\sigma(0)$ will be very large when $\omega=0$ is inside the conduction band and $\mathrm{Im}\,M_{2,\sigma}^{\mathrm{at}}(0)\sim 0$. The physical reason for this different behavior at very low T is the small number of carriers when $\omega=0$ is inside the gap, and the reduced number of scattering processes for the c electrons when $\omega=0$ is inside the band.

To analyze $M_{2,\sigma}^{\mathrm{at}}(z)$ we notice from Eq. (13) that $G_{ff,0\sigma}^{\mathrm{at}}(z)$ is real when $\eta\equiv \mathrm{Im}\,[z]\to 0$, except at its only singularities on the real axis, that are the poles at $z=u_j$. It is then clear from Eq. (14) that $M_{2,\sigma}^{\mathrm{at}}(z)$ is real on the real axis of the z complex plane except at the real solutions of $(\omega-E_0^a+\mu)-|V|^2G_{ff,0\sigma}^{\mathrm{at}}(\omega)=0$, where it would have poles with $\mathrm{Im}\,M_{2,\sigma}^{\mathrm{at}}(z)\neq 0$ in their neighborhood [the real values $M_{2,\sigma}^{\mathrm{at}}(u_j)=-(u_j-E_0^a+\mu)/|V|^2$ are taken at the poles u_j of $G_{ff,0\sigma}^{\mathrm{at}}(z)$]. One should then make all the calculations at a finite η and afterward take $\eta\to 0$.

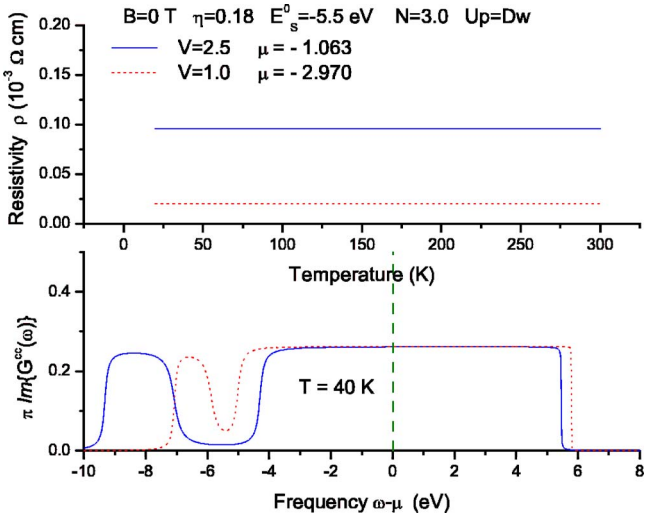

FIG. 11. (Color online) (a) Hybridized bands of free electrons, calculated for $V=2.5$ and $V=1.0$ and the same value of the remaining parameters (and in particular of $\eta_a=0.18$). We use $N=3$ so that μ is well inside the conduction band, and consider a paramagnetic phase at all T. (b) The resistivity as a function of T for the two values of V, confirming that the basic scattering mechanism in our calculation of $\sigma(T)$ is the hybridization.

The extreme sharpness of the structure of $\mathrm{Im}\,M_{2,\sigma}^{\mathrm{at}}(z)$ is a consequence of the atomic approximation employed, and to alleviate this character we have added an extra imaginary part $\eta_a=|\eta_a|\mathrm{sgn}(\mathrm{Im}[z])$ to its argument: $M_{2,\sigma}^{\mathrm{at}}(z)\Rightarrow M_{2,\sigma}^{\mathrm{at}}(\omega+i\eta_a)$, so that the real poles of this quantity become Lorentzians that somehow mimic the effect of the bandwidth. In some special situations this procedure can change substantially the value of $M_{2,\sigma}^{\mathrm{at}}(z)$ at the Fermi surface, and therefore the value of the conductivity (e.g., see Fig. 7 in Ref. 13).

It seems clear that the basic scattering mechanism in our calculation of $\sigma(T)$ is the hybridization, because the otherwise free conduction electrons are scattered by the localized f electrons through this interaction. This is apparent if we notice that the relaxation effects are described by the imaginary part of the usual self-energy $\Sigma_{cc,\sigma}(\mathbf{k},z)$, defined through

$$G_{cc,\sigma}(\mathbf{k},z)=-\{z-\varepsilon(\mathbf{k})-\Sigma_{cc,\sigma}(\mathbf{k},z)\}^{-1}, \qquad \text{(B1)}$$

and that the exact relation $\Sigma_{cc,\sigma}(\mathbf{k},z)=-|V(\mathbf{k})|^2M_{2,\sigma}^{\mathrm{eff}}(\mathbf{k},z)$ follows from Eq. (10). The relaxation mechanism of the c electrons is then provided by the hybridization, and the self-energy is independent of $\mathbf{k}$ in our approximation: $\Sigma_{cc,\sigma}(z)=-|V|^2M_{2,\sigma}^{at}(z)$.

Addition of $i\eta_a$ to the argument of $M_{2,\sigma}^{\mathrm{at}}(z)$ leads to effects similar to those already discussed by Mutou and Hirashima[33] through "introducing a small imaginary part Γ to the conduction electrons," i.e., replacing $z=i\,\omega$ by $z+i\,\Gamma\,\mathrm{sgn}(\omega)$ in the

GFs $G_{ff,\sigma}(\mathbf{k},z)$ and $G_{cc,\sigma}(\mathbf{k},z)$. Their justification is the existence in real systems of scattering processes due to phonons and impurities, and we should also consider these mechanisms as contributing to the $i\eta_a$. Within this interpretation one could also consider a temperature dependence of η_a, but we have not implemented this change in the present calculation.

At this point one might wonder whether the relaxation effects, that we obtain when we add the imaginary part η_a are all due to the scattering mechanisms of the imperfections and not to the effect of the hybridization. The argument would be that the carriers are the hybridized electrons, and that this potential should not introduce any scattering effect because we are dealing with Bloch electrons in a perfect lattice. Czycholl and Leder[32] already addressed this point [cf. text around their Eq. (17)], stating that, "it is completely unjustified to use a current operator of the form

$$j = e\sum_{\sigma}\sum_{\alpha=1,2}\sum_{\mathbf{k}}\frac{\partial E_{\alpha\mathbf{k}}}{\partial \mathbf{k}}\alpha^{+}_{\mathbf{k}\sigma}\alpha_{\mathbf{k}\sigma}$$

where $|\alpha_{\mathbf{k}\sigma}\rangle$ denotes the eigenstates of the one particle part of the Hamiltonian." Rather than elaborate on this statement, we shall give an independent argument.

To avoid the temperature changes of shape that are usual in correlated bands of electrons, we consider two hybridized bands of free electrons. In the lower part of Fig. 11 we show the bands corresponding to $V=2.5$ eV and $V=1.0$ eV and with the same value of all the other parameters (and in particular of η_a). Their shape is independent of T, and we have adjusted the chemical potential μ so that the total number of electrons is $N=3.0$, so that μ is well inside the conduction band. We have also assumed a paramagnetic phase at all T, so the two bands with spin up and spin down electrons are identical. In the upper part of the figure we plot the resistivity of the two bands as a function of T, which clearly shows the dependence of the resistivity with V, confirming that the basic scattering mechanism in our calculation of $\sigma(T)$ is the hybridization. The use of free electrons instead of correlated ones does not introduce any difference in the present discussion.

[1] A. P. Ramirez and M. A. Subramanian, Science **277**, 546 (1997).
[2] S. K. Mishra and S. Satpathy, Phys. Rev. B **58**, 7585 (1998).
[3] D. J. Singh, Phys. Rev. B **55**, 313 (1997).
[4] Y. Shimakawa, Y. Kubo, N. Hamada, J. D. Jorgensen, Z. Hu, S. Short, M. Nohara, and H. Takagi, Phys. Rev. B **59**, 1249 (1999).
[5] N. P. Raju, J. E. Greedan, and M. A. Subramanian, Phys. Rev. B **49**, 1086 (1994).
[6] Y. Shimakawa, Y. Kubo, and T. Manako, Nature (London) **379**, 1086 (1996).
[7] B. Martínez, R. Senis, J. Fontcuberta, X. Obradors, W. Cheikh-Rouhou, P. Strobel, C. Bougerol-Chaillout, and M. Pernet, Phys. Rev. Lett. **83**, 2022 (1999).
[8] S. W. Cheong, H. Y. Wang, B. Batlogg, and L. W. Rupp, Solid State Commun. **98**, 163 (1996).
[9] H. Imai, Y. Shimakawa, Y. V. Sushko, and Y. Kubo, Phys. Rev. B **62**, 12190 (2000).
[10] Y. V. Sushko, Y. Kubo, Y. Shimakawa, and T. Manako, Physica B **259-261**, 831 (1999).
[11] M. D. Nuñez-Regueiro and C. Lacroix, Phys. Rev. B **63**, 014417 (2000).
[12] C. I. Ventura and B. Alascio, Phys. Rev. B **56**, 14533 (1997).
[13] M. E. Foglio and M. S. Figueira, Phys. Rev. B **60**, 11361 (1999).
[14] Y. Shimakawa, Y. Kubo, T. Manako, Y. V. Sushko, D. N. Argyriou, and J. D. Jorgensen, Phys. Rev. B **55**, 6399 (1997).
[15] H. Okamura, T. Koretsune, M. Matsunami, S. Kimura, T. Nanba, H. Imai, Y. Shimakawa, and Y. Kubo, Phys. Rev. B **64**, 180409(R) (2001).
[16] H. Schweitzer and G. Czycholl, Phys. Rev. Lett. **67**, 3724 (1991).
[17] A. L. Fetter and J. D. Walecka, *Quantum Theory of Many-Particle Systems* (McGraw-Hill, New York, 1971).
[18] J. Hubbard, Proc. R. Soc. London, Ser. A **296**, 82 (1966).
[19] M. S. Figueira, M. E. Foglio, and G. G. Martinez, Phys. Rev. B **50**, 17933 (1994).
[20] J. W. Negele and H. Orland, *Quantum Many-Particle Systems* (Addison-Wesley, New York, 1988).
[21] D. N. Zubarev, Sov. Phys. Usp. **3**, 320 (1960).
[22] W. Metzner, Phys. Rev. B **43**, 8549 (1991).
[23] M. E. Foglio and M. S. Figueira, Phys. Rev. B **62**, 7882 (2000).
[24] P. Fulde, Solid State Phys. **41**, 1 (1988).
[25] A. C. Hewson, *The Kondo Problem to Heavy Fermions* (Cambridge University Press, Cambridge, 1993).
[26] G. G. Martinez Pino, Ph.D. thesis, Universidade Estadual de Campinas, Campinas, SP, Brazil, 1989.
[27] B. Alascio, R. Allub, and A. A. Aligia, Z. Phys. B **36**, 37 (1979).
[28] R. Kubo, J. Phys. Soc. Jpn. **12**, 570 (1957).
[29] G. D. Mahan, *Many-Particle Physics* (Plenum, New York, 1990).
[30] H. Schweitzer and G. Czycholl, Phys. Rev. Lett. **67**, 3724 (1991).
[31] A. Khurana, Phys. Rev. Lett. **64**, 1990 (1990).
[32] G. Czycholl and H. J. Leder, Z. Phys. B: Condens. Matter **44**, 59 (1981).
[33] T. Mutou and D. S. Hirashima, J. Phys. Soc. Jpn. **63**, 4475 (1994).
[34] T. Pruschke, D. L. Cox, and M. Jarrell, Phys. Rev. B **47**, 3553 (1993).
[35] R. Consiglio and M. A. Gusmão, Phys. Rev. B **55**, 6825 (1997).
[36] E. Muller Hartmann, Z. Phys. B: Condens. Matter **74**, 507 (1989).
[37] M. A. Subramanian, B. H. Toby, A. P. Ramirez, W. J. Marshall, A. W. Sleight, and G. H. Kwei, Science **273**, 81 (1996).
[38] G. H. Kwei, C. H. Booth, F. Bridges, and M. A. Subramanian, Phys. Rev. B **55**, R688 (1997).
[39] M. J. Rozenberg, G. Kotliar, and H. Kajueter, Phys. Rev. B **54**, 8452 (1996).
[40] D. Baeriswyl, C. Gros, and T. M. Rice, Phys. Rev. B **35**, 8391 (1987).
[41] P. Majundar and P. Littlewood, Phys. Rev. Lett. **81**, 1314 (1998).
[42] P. Majundar and P. Littlewood, Nature (London) **395**, 479 (1998).
[43] M. J. Calderon, L. Brey, and P. Littlewood, Phys. Rev. B **62**,

3368 (2000).
[44] L. G. L. Wegener and P. Littlewood, Phys. Rev. B **66**, 224402 (2002).
[45] M. L. Fisher and J. S. Langer, Phys. Rev. Lett. **20**, 665 (1968).
[46] R. L. Carlin, *Magnetochemistry* (Springer, 1986).
[47] The properly assigned values correspond to the ions with the orbital angular momentum quenched: They are 3.87 μ_B for Mn^{4+} and 2.83μ_B for Mn^{5+}. Typical values observed experimentally (Ref. 46) are 3.7 μ_B−3.9 μ_B for Mn^{4+} and 2.8 μ_B −2.9 μ_B for Mn^{5+}.